A&A 592, A99 (2016)
DOI: 10.1051/0004-6361/201527650


Astronomy & Astrophysics

# Irradiation of nitrogen-rich ices by swift heavy ions

## Clues for the formation of ultracarbonaceous micrometeorites

B. Augé[1,2], E. Dartois[2], C. Engrand[3], J. Duprat[3], M. Godard[3], L. Delauche[3], N. Bardin[3], C. Mejía[1,4], R. Martinez[1,5], G. Muniz[1], A. Domaracka[1], P. Boduch[1], and H. Rothard[1]

[1] Centre de Recherche sur les Ions, les Matériaux et la Photonique CIMAP (CEA/CNRS/ENSICAEN/Université de Caen Normandie), Boulevard Henri Becquerel, BP 5133, 14070 Caen Cedex 05, France
e-mail: auge@ganil.fr
[2] Institut d'Astrophysique Spatiale, UMR 8617 CNRS-Univ. Paris-Sud, Université Paris-Saclay, Bâtiment 121, Univ. Paris-Sud, 91405 Orsay Cedex, France
[3] Centre de Sciences Nucléaires et de Sciences de la Matière, UMR 8609 CNRS/IN2P3-Univ. Paris-Sud, Université Paris-Saclay, Bâtiment 104, 91405 Orsay Campus, France
[4] Departamento de Física, Pontifícia Universidade Católica do Rio de Janeiro, Rua Marquês de São Vicente 225, 22453-900 Rio de Janeiro, RJ, Brazil
[5] Departamento de Física, Universidade Federal do Amapá, Rod. JK Km. 02, Jardim Marco Zero, 22453-900 Macapá, Brazil

Received 27 October 2015 / Accepted 27 May 2016

**ABSTRACT**

*Context.* Extraterrestrial materials, such as meteorites and interplanetary dust particles, provide constraints on the formation and evolution of organic matter in the young solar system. Micrometeorites represent the dominant source of extraterrestrial matter at the Earth's surface, some of them originating from large heliocentric distances. Recent analyses of ultracarbonaceous micrometeorites recovered from Antarctica (UCAMMs) reveal an unusually nitrogen-rich organic matter. Such nitrogen-rich carbonaceous material could be formed in a $N_2$-rich environment, at very low temperature, triggered by energetic processes.
*Aims.* Several formation scenarios have been proposed for the formation of the N-rich organic matter observed in UCAMMs. We experimentally evaluate the scenario involving high energy irradiation of icy bodies subsurface orbiting at large heliocentric distances.
*Methods.* The effect of Galactic cosmic ray (GCR) irradiation of ices containing $N_2$ and $CH_4$ was studied in the laboratory. The $N_2$-$CH_4$ (90:10 and 98:2) ice mixtures were irradiated at 14 K by 44 MeV $Ni^{11+}$ and 160 MeV $Ar^{15+}$ swift heavy ion beams. The evolution of the samples was monitored using in-situ Fourier transform infrared spectroscopy. The evolution of the initial ice molecules and new species formed were followed as a function of projectile fluence. After irradiation, the target was annealed to room temperature. The solid residue of the whole process left after ice sublimation was characterized in-situ by infrared spectroscopy, and the elemental composition was measured ex-situ.
*Results.* The infrared bands that appear during irradiation allow us to identify molecules and radicals (HCN, $CN^-$, $NH_3$, ...). The infrared spectra of the solid residues measured at room temperature show similarities with that of UCAMMs. The results point towards the efficient production of a poly-HCN-like residue from the irradiation of $N_2$-$CH_4$ rich surfaces of icy bodies. The room temperature residue provides a viable precursor for the N-rich organic matter found in UCAMMs.

**Key words.** astrochemistry – Oort Cloud – cosmic rays – meteorites, meteors, meteoroids – methods: laboratory: solid state

## 1. Introduction

Interplanetary dust particles (IDPs) and meteorites provide information about primitive solar system matter and its chemical evolution. Micrometeorites recovered in Antarctic snow (AMMs) near the CONCORDIA station (Duprat et al. 2007) or near Dome Fuji (Nakamura et al. 1999; Ebihara et al. 2013) provide a unique source of pristine interplanetary dust particles. Among the fraction of AMMs that underwent a minimal weathering at atmospheric entry, a few percent are characterized by a very large carbon content (Nakamura et al. 2005; Duprat et al. 2010). The carbonaceous phase of these so-called ultracarbonaceous Antarctic micrometeorites (UCAMMs) is an organic matter that exhibits extreme deuterium excesses (Duprat et al. 2010). These particles are different from classical IDPs and AMMs and represent a new class of interplanetary material (Nakamura et al. 2005; Duprat et al. 2010; Dobrică et al. 2011, 2012; Yabuta et al. 2012; Engrand et al. 2015). Analysis by Raman and infrared absorption spectroscopy of these UCAMMs revealed that they contain nitrogen-rich organic matter with atomic N/C up to ~0.15 (Dartois et al. 2013; Dobrică et al. 2011).

An important issue is how organic matter of meteorites, in general, and of UCAMMs, in particular, is formed. The first infrared spectroscopy studies of insoluble organic matter (IOM), extracted from primitive carbonaceous chondrite meteorites suggested that their chemical composition was similar to that observed in interstellar medium (e.g. Ehrenfreund et al. 1991 and onwards citations). However, these first studies were limited to the 3.4 $\mu$m spectral window. The extension to the full infrared spectral domain, covered later on by space telescopes, showed that the spectroscopic signatures of the meteorite organic extract is not fully similar to that of interstellar medium (ISM) carbonaceous matter. In particular, studies in the atmosphere-free mid-infrared region showed that many spectroscopic signatures of the IOM in the 5 to 10 $\mu$m window are different from that of hydrogenated carbon dust observed in the ISM

(Kebukawa et al. 2011; Orthous-Daunay et al. 2013, lower spectrum in Fig. 1). The IOM structure in the Orgueil meteorite and the labile fraction in CM chondrites (Kitajima et al. 2002; Remusat et al. 2007, right structure Fig. 1; Derenne & Robert 2010) both possess a chemical network that is different from that of ISM components. The IOM absorption features absent in the spectra observed in diffuse ISM dust are mainly related to the presence of oxygen heteroatoms in the organic network. In the ISM dust, there is no evidence for the incorporation of such oxygen or nitrogen heteroatoms. In contrast, the UCAMM infrared spectra are characterized by absorption bands related to nitrogen heteroatoms (Dartois et al. 2013). The evolution of the carbonaceous phase from diffuse to dense medium is still poorly constrained. It is possible that the ISM carbonaceous matter contains early precursors that were subsequently modified at various stages during evolution from the dense molecular cloud core to the protoplanetary disk and, eventually, later on during the meteorite formation process. Laboratory experiments allow the replication of space energetic environments to which the ices are exposed and to produce residues after slow sublimation of the ice. However, residues both obtained at room temperature (e.g. Muñoz Caro et al. 2004; Nuevo et al. 2006) and exposed directly to cosmic radiation in space (e.g. EURECA experiment, Greenberg et al. 1995) do not match the residues of the IOM from meteorites. Moreover, the macromolecular organics expected to be formed from ice mantles processed in the laboratory under simulated dense cloud conditions are distinct from that of IOM. Such laboratory residues may be considered a possible starting (or precursor) material, provided that the subsequent evolutionary pathways, such as thermal metamorphism or strong post-formation irradiation, can lead to further evolution (Muñoz Caro & Dartois 2013). Such an evolution may eventually produce the IOM found in carbonaceous chondrites meteorites, however, it is clearly different from the N-rich organic matter with lower O content found in UCAMMs and some IDPs. The UCAMM organic matter may have formed early in the history of the solar system from the protosolar cloud dust grains. Alternatively, this organic matter may have endured more recent evolution on its parent body. Nevertheless, the mere formation of an organic material with spectral characteristics close to that observed in UCAMMs, i.e. in which up to several tens of percent of N have been incorporated and with low amounts of oxygen, requires the presence of a carbonaceous precursor and energetic processes in a N-dominated environment (Dartois et al. 2013; Ong et al. 1996; Hammer et al. 2000; Rodil et al. 2001; Quirico et al. 2008; Gerakines et al. 2004; Moore et al. 2003; Hudson et al. 2001). Such conditions are gathered at the surface of some objects, which are orbiting at large heliocentric distances, beyond the trans-Neptunian region, with $N_2$-rich icy surfaces (Schaller & Brown 2007; Levi & Podolak 2011). The energetic process can indeed be provided by irradiation with cosmic rays and/or visible-ultraviolet (VUV) photons (Cooper et al. 2003). Three different scenarios have been proposed to explain the formation of UCAMMs in Dartois et al. (2013). We provide hereafter a brief summary of these scenarios and implications; see this article and the references therein for further details.

Thus UCAMMs may be (1) a heritage from the protoplanetary disk; (2) a fragment from a large Kuiper belt object (KBO); or (3) a residue of irradiated ices formed on a comet-parent body in the Oort cloud. However, the macromolecular residues formed according to the first irradiation scenario should be different in composition from that found in UCAMMs (Dartois et al. 2013). Indeed because of the presence of abundant water ice in protoplanetary disk and dense interstellar environments, the matter recovered should present some features related to a higher amount of incorporated oxygen atoms in the solid network, whereas the organic matter of UCAMMs exhibits a low O/C ratio. In the last two scenarios, the formation of nitrogen-rich organic matter in the outermost regions of the solar system can be explained, since nitrogen and methane rich ices are condensed at the surface of icy bodies (Protopapa et al. 2016; Grundy et al. 2016; Licandro et al. 2006; Lorenzi et al. 2015; Cruikshank et al. 2015), and water ice is buried and protected from the ambient radiation fields. These scenarios are favoured to explain the formation of N-rich organic matter because of the expected final organic matter composition and the volume of irradiated material. However, experimental constraints on irradiation times corresponding to these locations in the solar system (e.g. Cooper et al. 2003) and on the volume of matter affected are needed to better distinguish the most fitting scenario. The third scenario permits the largest affected volume, combining a region where icy bodies are exposed to higher energy cosmic rays penetrating deeper in the subsurface, with potentially more small icy bodies with a $N_2$-$CH_4$ rich subsurface than in the second scenario.

Several publications have reported experimental studies on ion bombardment of interplanetary ice analogues with $N_2$ and $CH_4$ included in the mixture (e.g. Gerakines et al. 2004; Moore et al. 2003; Hudson et al. 2001; Barrata et al. 2015). These experiments were mainly performed at low ion energies, less than a few MeV. Here, we report on the effect of swift heavy ions corresponding to GCR (Galactic cosmic ray) irradiation of a typical large KBO or Oort cloud icy body surface. We thus evaluate experimentally UCAMM formation scenarios proposed in Dartois et al. (2013) and discuss the astrophysical implications for the formation and evolution of the organic matter observed in UCAMMs

## 2. Experiments and methods

### 2.1. Experiments

The irradiation experiments were performed at the heavy ion accelerator Grand Accélérateur National d'Ions Lourds (GANIL; Caen, France) with $Ni^{11+}$ (44 MeV) at the IRRSUD beam line and $Ar^{15+}$ (160 MeV) at the SME beam line. The experimental procedures have been reported before (Pilling et al. 2010; Seperuelo Duarte et al. 2009). The CASIMIR set-up (Chambre d'Analyse par Spectroscopie Infrarouge des Molécules IRadiées, Fig. 1), which can be mounted on both of these beam lines, is a high vacuum chamber ($\sim 10^{-8}$ mbar) with a rotatory platform holding an infrared (IR) transparent ZnSe substrate. This substrate can be cooled down with a closed-cycle helium cryostat to a temperature of about 14 K, allowing a controlled substrate temperature from 14 K to 300 K. The irradiation beam lines are equipped with a beam sweeping device, which provides a homogeneously irradiated surface. In the present experiments, we condensed a gaseous mixture of $N_2$ and $CH_4$ onto the ZnSe substrate at 14 K. We used two $N_2$-$CH_4$ mixtures, the first with a nominal concentration of 1.99% of methane (98:2) and the second with 9.98% of methane (90:10). Both were acquired from Air Liquide and used as received (see Table 1). Such mixtures are representative of the main composition for methane and nitrogen-rich surfaces of the dwarf planet Pluto (Cruikshank et al. 2015; Grundy et al. 2016) and are also relevant for some surfaces on other dwarf planets (e.g. Eris, Makemake, see Licandro et al. 2006; Lorenzi et al. 2015). Thousands of smaller objects in the Kuiper belt and Oort cloud regions should possess the same kind

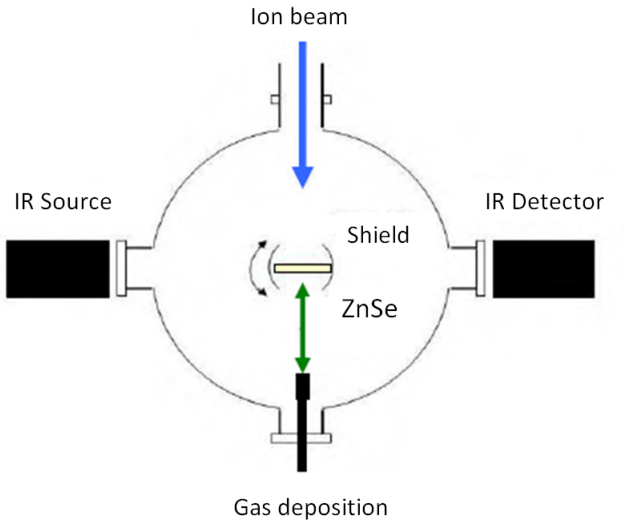


**Fig. 1.** Experimental CASIMIR set-up. The gas is injected and condensed on a ZnSe window. This window can be rotated to be exposed to the ion beam or to the Fourier Transformed Infrared (FTIR) beam.

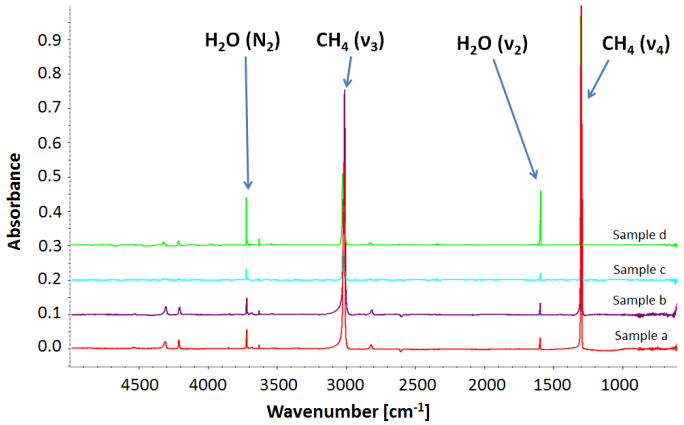


**Fig. 2.** Infrared spectra of samples a to d. Samples a and b were deposited using a (90:10) $N_2$-$CH_4$ mixture, and samples c and d using a (98:2) mixture. Spectra were shifted for clarity. Small amounts of water contamination are present in the spectra. The major bands are identified, see text and Table 1 for details.

of surface composition, but their spectra are not yet accessible owing to their magnitudes that are too low.

The substrate on the cold head can be rotated into three positions: to deposit the ice, to irradiate it, or to record IR spectra at normal incidence in transmission. Spectra were recorded in-situ with a FTIR spectrometer (Nicolet Magna 750) before and during irradiation at different fluences, and at different temperature steps during heating. The slow warming up was performed from 14 K to 300 K with a ramp at ~0.2 K min$^{-1}$ for $T \leq 70$ K (to allow a gentle non-processed $N_2$ and $CH_4$ sublimation) and with a 1−1.5 K min$^{-1}$ ramp for $T > 70$ K. When the sample reached 300 K, a final IR spectrum was recorded. The chamber was then opened to dismount the ZnSe window covered with the residue. The residue was kept under primary dry vacuum for further ex-situ analysis. Electron microprobe measurements (Cameca SX100) were performed at the Pierre and Marie Curie University (Paris VI, CAMPARIS) at 10 kV to measure the atomic N/C ratio of the residues. One of the residues was also post-annealed under primary vacuum up to 600 K to observe the evolution of the organic matter composition, as monitored by FTIR. The residue was placed under dynamic primary vacuum in an evacuated quartz tube placed into an oven, and the temperature increased to 600 K at 5 K min$^{-1}$. The sample was maintained at 600 K during 30 min and then removed from the oven. The sample was allowed to cool down under vacuum at room temperature before any further measurement.

### 2.2. Ice samples

Figure 2 presents the spectra of four different deposited $N_2$-$CH_4$ ices. Two of these (sample a and sample b) were prepared with a (90:10) mixture with a thickness of 8.4 and 9.9 $\mu$m, respectively. The others (sample c and sample d) were prepared with a (98:2) mixture with a thickness of 10 and 20 $\mu$m, respectively. The thickness was determined using residual interference fringes measured on the IR spectra as summarized in Table 1. The IR spectra of freshly deposited ice films (Fig. 2) reveal different absorption bands at 4550, 4310, 4210, 3010, 2820, and 1305 cm$^{-1}$, which can all be assigned to the $CH_4$ molecule (Gerakines et al. 2005). Other bands observed at 3720, 3635, and 1600 cm$^{-1}$ correspond to small amounts of water residual pollution trapped into the $N_2$ matrix (Bentwood et al. 1980) whereas $N_2$ is IR inactive. This water comes from a residual gas contamination in the injection chamber.

The deposited ice column density can be calculated from

$$N = \frac{1}{A} \int_{\nu_1}^{\nu_2} \tau(\nu)\, \mathrm{d}\nu \qquad (1)$$

where $N$ is the column density in molecules cm$^{-2}$, $\tau(\nu)$ the frequency dependent optical depth of the considered infrared band and $A$ the integrated band strength in cm molecule$^{-1}$. The band strengths we adopted for the different molecules can be found in Escobar et al. (2014), Moore et al. (2003) and Gerakines et al. (2005). The effective initial composition was obtained using the methane band at 3010 cm$^{-1}$ and the water band at 1600 cm$^{-1}$ as reference. The adopted band strength values are $A_{CH_4} = 6{\times}10^{-18}$ and $A_{H_2O} = 1.2 \times 10^{-17}$ cm molecule$^{-1}$, respectively. Table 1 summarizes the mixtures composition for the deposited ice films, estimated sample thickness, and molecule column densities, taking the presence of $H_2O$ into account.

The two ice films with 10% of methane (samples a and b) were irradiated with $Ni^{11+}$ at 44 MeV and the ice films with 2% of methane (samples c and d) with $Ar^{15+}$ at 160 MeV. The beam parameters are given in Table 1. The samples were irradiated until a total fluence of $1.0 \times 10^{13}$, $3 \times 10^{13}$, $3.4 \times 10^{12}$, and $2.2 \times 10^{13}$ ions cm$^{-2}$, for samples a to d, respectively. The total dose deposited in the ices (given in Table 1) was calculated using the SRIM code (Ziegler et al. 2010), assuming an ice density of 0.94 g cm$^{-3}$ (Satorre et al. 2008).

## 3. Results

### 3.1. Irradiation of the ice mixtures

Infrared spectra taken before, during and at the end of the irradiation for the four samples are shown in Figs. 3−6. These spectra clearly show the decrease of the $CH_4$ bands related to the destruction of this molecule under irradiation. Figure 6 exhibits a strong water ice contamination at the end of the experiment as shown by the broad water ice bands around 3280 cm$^{-1}$ and 1600 cm$^{-1}$. For this particular sample (sample d), the beam was

**Table 1.** Deposited molecules.

| Sample | Conc.[a] $N_2$:$CH_4$ | Thickness[b] [$\mu$m] | Molecule[c] | $N$[d] [cm$^{-2}$] | Beam | Energy [MeV] | $S_e$[e] [keV $\mu$m$^{-1}$] | Fluence [ions cm$^{-2}$] | Dose[f] [eV molecule$^{-1}$] |
|---|---|---|---|---|---|---|---|---|---|
| a | 90:10 | 8.4 ± 0.4 | $CH_4$ | $1.7 \times 10^{18}$ | $^{58}Ni^{11+}$ | 44 | 3794 | $1.0 \times 10^{13}$ | 18 |
| | | | $H_2O$ | $1.6 \times 10^{16}$ | | | | | |
| b | 90:10 | 9.9 ± 0.5 | $CH_4$ | $1.5 \times 10^{18}$ | $^{58}Ni^{11+}$ | 44 | 3794 | $3.0 \times 10^{13}$ | 54 |
| | | | $H_2O$ | $1.6 \times 10^{16}$ | | | | | |
| c | 98:2 | 10.0 ± 0.6 | $CH_4$ | $2.6 \times 10^{17}$ | $^{40}Ar^{15+}$ | 160 | 1617 | $3.4 \times 10^{12}$ | 3 |
| | | | $H_2O$ | $8.3 \times 10^{15}$ | | | | | |
| d | 98:2 | 20 ± 2 | $CH_4$ | $6.3 \times 10^{17}$ | $^{40}Ar^{15+}$ | 160 | 1617 | $2.2 \times 10^{13}$ | 18 |
| | | | $H_2O$ | $4.4 \times 10^{16}$ | | | | | |

**Notes.** [(a)] Concentration given by Air Liquide. [(b)] The thickness is estimated from the interference fringes period via the formula $e \approx 1/2n\Delta\nu$, where $e$ is the thickness, $n$ the refractive index of the ice film, and $\Delta\nu$ the period of interference fringes. [(c)] Taking into account the water pollution. [(d)] The calculated water contamination is about 1−7% with respect to $CH_4$. [(e)] Calculated with SRIM (Ziegler et al. 2010), assuming an ice density of 0.94 g cm$^{-3}$ (Satorre et al. 2008). [(f)] $D = F \times S_e/\rho$, where F is the ion fluence, $S_e$ its electronic stopping power, and $\rho$ the target density.

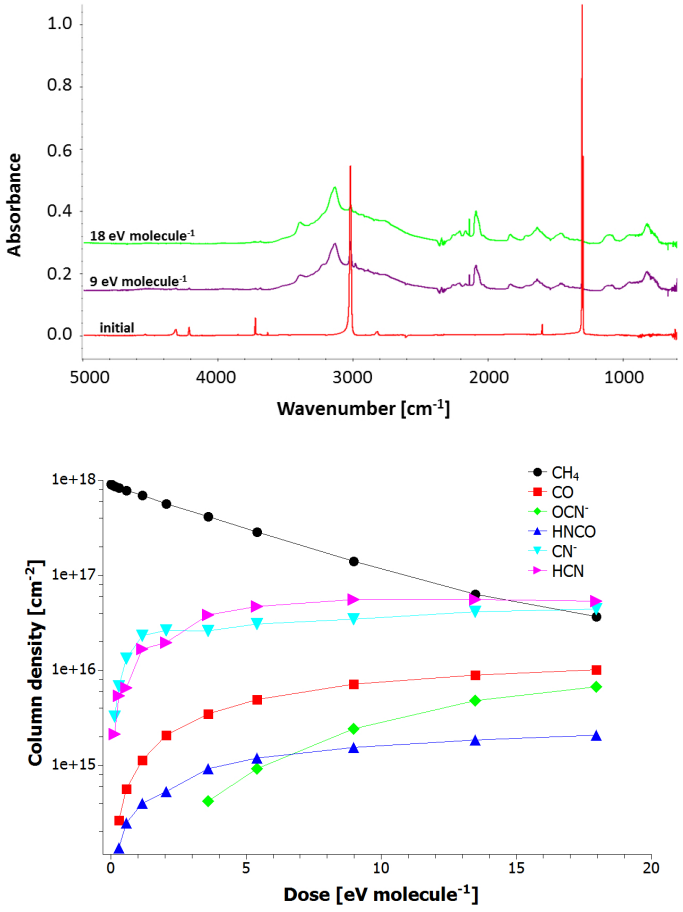


**Fig. 3.** Sample a: IR spectrum from 5000 to 600 cm$^{-1}$ of $N_2$:$CH_4$; 9.4 $\mu$m thickness (*top*). *From bottom to top*, initial deposited ice sample (red), after a fluence of $5\times10^{12}$ ions cm$^{-2}$ (purple) and $1\times10^{13}$ ions cm$^{-2}$ (green). The final dose is 18 eV molecule$^{-1}$. Spectra were shifted for clarity. Evolution of the column density of selected molecules in the sample during the irradiation as a function of the deposited dose (*bottom*).

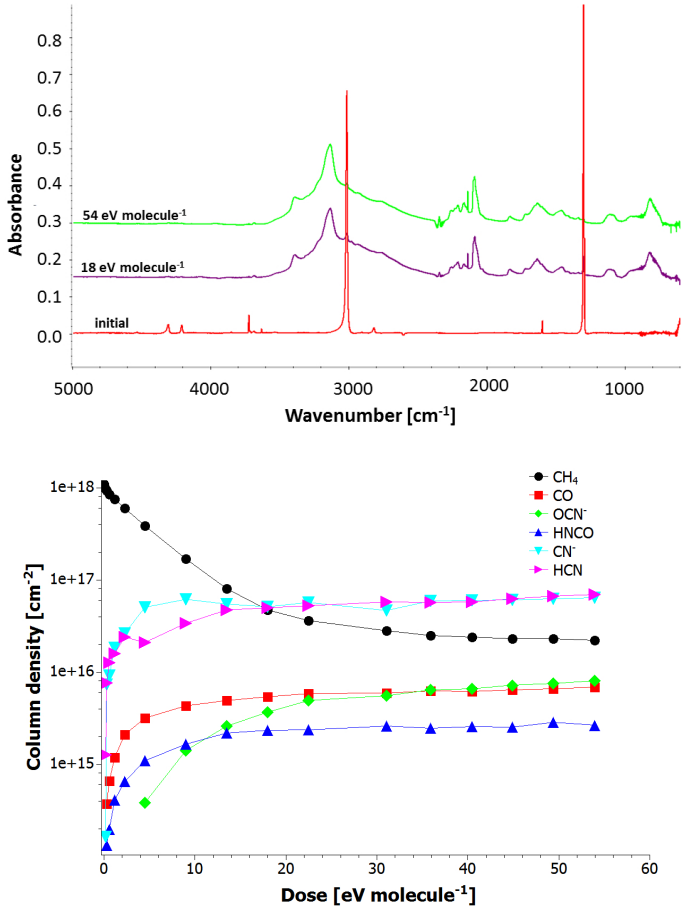


**Fig. 4.** Sample b: IR spectrum from 5000 to 600 cm$^{-1}$ of $N_2$:$CH_4$; 9.2 $\mu$m thickness (*top*). *From bottom to top*, initial deposited ice sample (red), after a fluence of $1\times10^{13}$ ions cm$^{-2}$ (purple) and $3\times10^{13}$ ions cm$^{-2}$ (green). The final dose is 54 eV molecule$^{-1}$. Spectra were shifted for clarity. Evolution of the column density of selected molecules in the sample during the irradiation as a function of the deposited dose (*bottom*).

stopped during 12 h as a result of a technical incident, and an important layering of water ice, accreted from the residual vacuum gas, occurred on top of the $N_2$-$CH_4$ film. Nevertheless the experiment was pursued immediately up to the final fluence when the beam was recovered. The water-ice deposition occurred at the surface of the ice mixture only, whereas the irradiation affected the whole bulk sample. Indeed, the range of the projectile (87 $\mu$m) is much larger than the target thickness (23 $\mu$m)

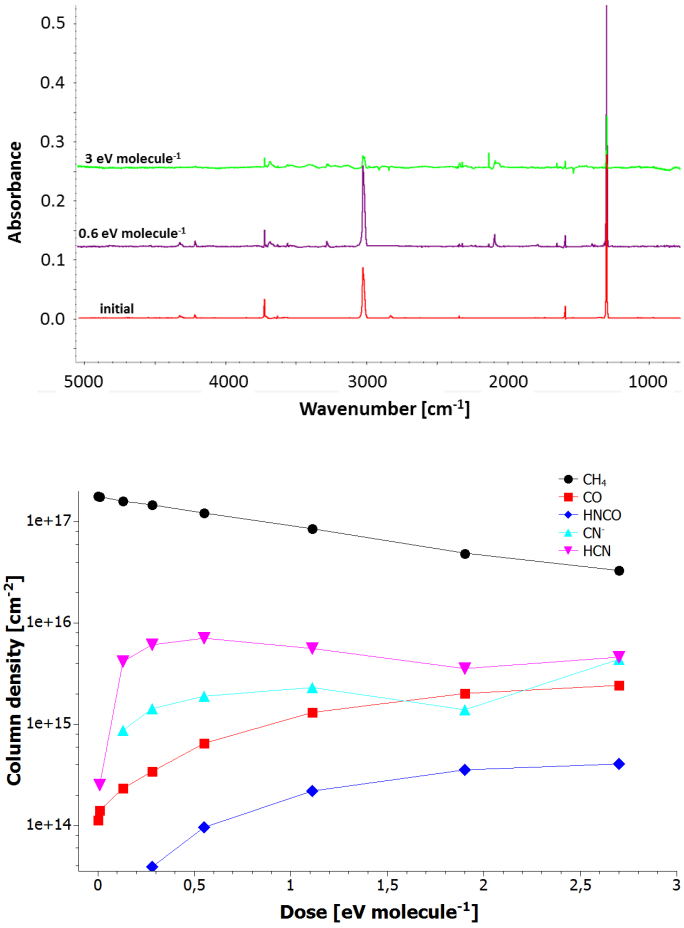


**Fig. 5.** Sample c: IR spectrum from 5000 to 600 $cm^{-1}$ of $N_2$:$CH_4$; 9.3 $\mu$m thickness (*top*). *From bottom to top*, initial deposited ice sample (red), after a fluence of $6.9 \times 10^{11}$ ions $cm^{-2}$ (purple) and $3.4 \times 10^{12}$ ions $cm^{-2}$ (green). The final dose is 3 eV $molecule^{-1}$, which is not enough to obtain a final spectra equivalent to those of other samples irradiated with higher doses. Spectra were shifted for clarity. Evolution of the column density of selected molecules in the sample during the irradiation as a function of the deposited dose (*bottom*).

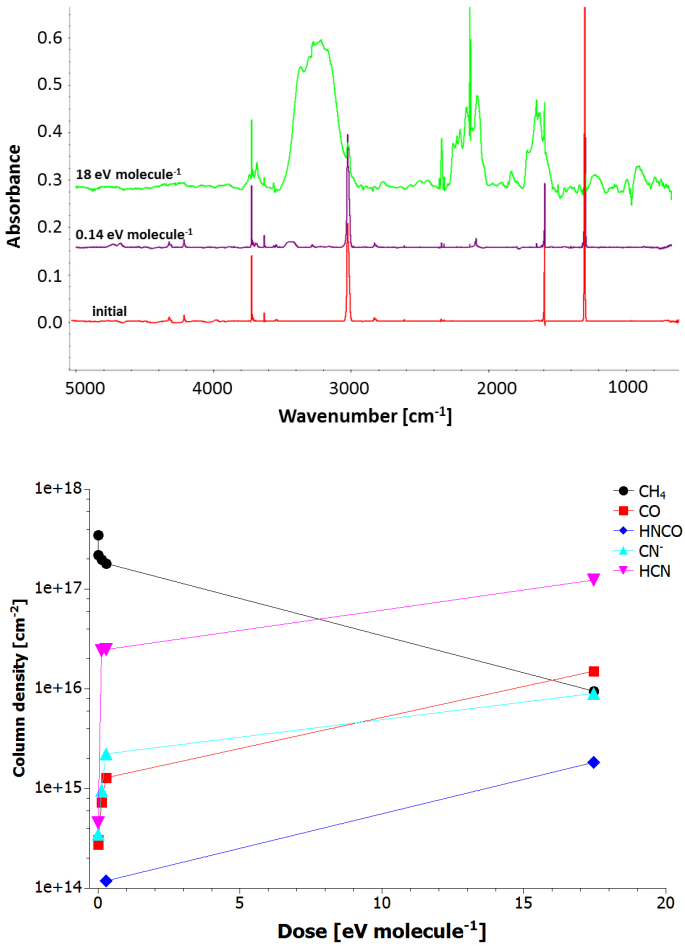


**Fig. 6.** Sample d: IR spectrum from 5000 to 600 $cm^{-1}$ of $N_2$:$CH_4$; 23 $\mu$m thickness (*top*). *From bottom to top*, initial deposited ice sample (red), after a fluence of $1.7 \times 10^{11}$ ions $cm^{-2}$ (purple) and $2.2 \times 10^{13}$ ions $cm^{-2}$ (green). The final dose is 18 eV $molecule^{-1}$. The final spectra indicates the presence of solid water. Spectra were shifted for clarity. Evolution of the column density of selected molecules in the sample during the irradiation as a function of the deposited dose (*bottom*). As a result of a technical incident, there is no point between 1 and 18 eV $molecule^{-1}$.

Numerous molecules can be formed as a result of the radiolysis of $CH_4$, $N_2$ (and $H_2O$). For high $CH_4$ concentration, molecules such as $C_2H_6$ are formed, as demonstrated by the features at 2975, 2950, and 2890 $cm^{-1}$. The production of $NH_3$ (1640 and 1100 $cm^{-1}$) or $NH_4^+$ (1470 $cm^{-1}$) is due to the destruction of $N_2$ combined with hydrogen coming from $CH_4$ or $H_2O$. The production of small amounts of CO (2140 $cm^{-1}$), $CO_2$ (2345 $cm^{-1}$), HNCO (2260 $cm^{-1}$), and $OCN^-$ (2170 $cm^{-1}$) results from the small water ice contamination, which is the only source of atomic oxygen in the ice mixtures. The feature around 2100 $cm^{-1}$ can be assigned to the formation of the $CN^-$ anion (2090 $cm^{-1}$) and HCN (2100 $cm^{-1}$). This molecule is also present at 3130, 1730, and 820 $cm^{-1}$.

The evolution of the column density of the most relevant molecules as a function of the deposited dose is reported in Figs. 3–6, and the infrared bands used to evaluate the column densities are listed in Table 2. After about 10 eV $molecule^{-1}$, the column densities of the main species do not further evolve substantially. This suggests that after such a dose the abundances of the irradiation-induced molecules reach a plateau, although the sample still evolves towards a refractory residue as seen through the presence of broad bands in the IR spectra. Also, we note that the initial composition does not significantly change the overall chemical evolution (Figs. 3, 4, and 6). The final spectra for irradiations starting with a 2% or a 10% methane ices are similar (see samples a, b, and d in Figs. 3, 4, and 6). To infer the relevance of the dose deposited in the ices, we exposed samples c to a total dose of only about 3 eV $molecule^{-1}$ (Fig. 5). The final spectra shows that the complex features around 3010 $cm^{-1}$ and 2200–2000 $cm^{-1}$ are much weaker than in other experiments, i.e. that the final dose is not sufficient to radiolyse enough $CH_4$ and $N_2$ to produce higher molecular weight species (see Fig. 5). Indeed at the end of the irradiation a substantial fraction of the initial methane is still present in the ice.

### 3.2. Annealing of irradiated ices to 300 K: Formation of organic residues

While transferring to the internal solar system, Oort cloud objects are heated. During this period, solar radiations sublimate particles from the surface of the object, allowing chemical

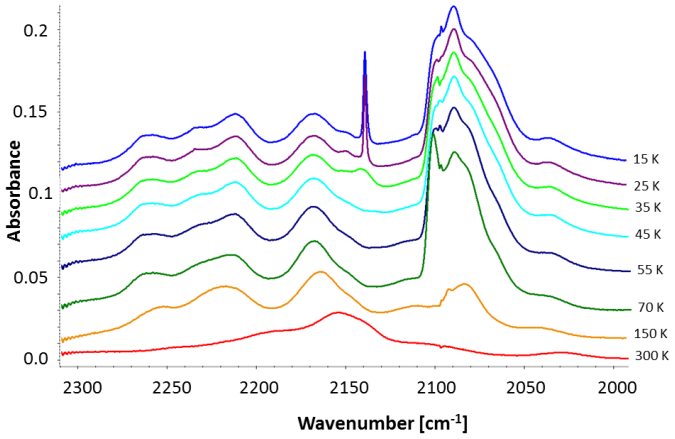


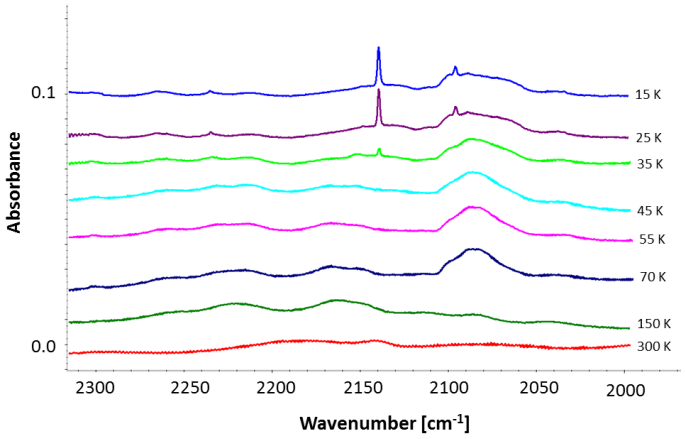


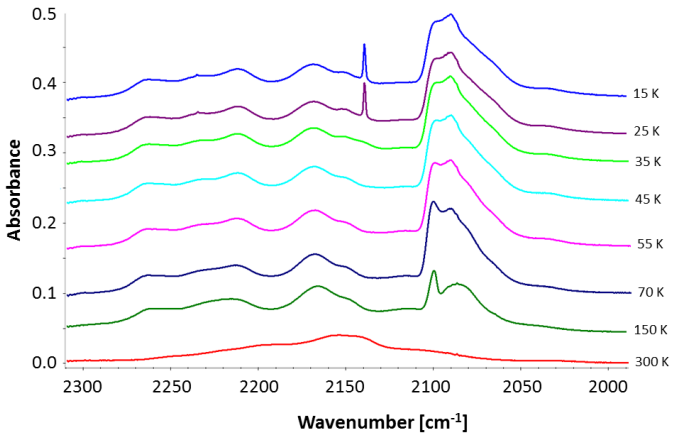


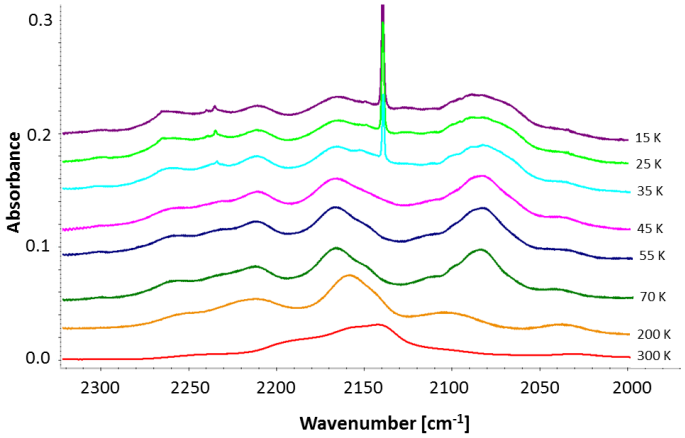


**Fig. 7.** Evolution of IR spectra between 2300 and 2000 $cm^{-1}$ during annealing of sample a to 300 K (*top*). Evolution of IR spectra between 2300 and 2000 $cm^{-1}$ during annealing of sample b to 300 K (*bottom*). Spectra were shifted for clarity.

**Fig. 8.** Evolution of IR spectra between 2300 and 2000 $cm^{-1}$ during annealing of sample c to 300 K (*top*). Evolution of IR spectra between 2300 and 2000 $cm^{-1}$ during annealing of sample d to 300 K (*bottom*). Spectra were shifted for clarity.

**Table 2.** Formed molecules or radical ions, only the most intense band is given for each species.

| Molecule | Band ($cm^{-1}$) | Reference |
|---|---|---|
| HCN | 2100 | Burgdorf et al. (2010) |
| $C_2H_6$ | 2975 | Bennett et al. (2006) |
| $C_2H_4N_4$ | 2210 | Gerakines et al. (2004) |
| $NH_3$ | 1100 | Pilling et al. (2010) |
| CO | 2140 | Palumbo & Strazzulla (1993) |
| HNCO | 2260 | Jheeta et al. (2013) |
| $NH_4^+$ | 1470 | Moon et al. (2010) |
| $CN^-$ | 2090 | Moore et al. (2003) |
| $OCN^-$ | 2170 | van Broekhuizen et al. (2004) |

modifications. This is the reason why, after each irradiation, the samples were slowly heated from 14 K to 300 K (annealing).

At the beginning, the temperature ramp was chosen to be slow enough (0.2 K $min^{-1}$) to allow for gentle diffusion and sublimation of the matrix and avoid explosive desorption of the ice matrix when nitrogen and methane sublimate (volcano effect).

For $T \geq 70$ K, the ramp was increased to 1 or 1.5 K $min^{-1}$. During annealing, infrared spectra were recorded to monitor the chemical evolution of the sample. The corresponding spectra in the 2300−2000 $cm^{-1}$ region are shown in Figs. 7 and 8 for the four samples.

The first species that sublimates is CO, as demonstrated by the disappearance of the 2140 $cm^{-1}$ band beyond 35 K. $CH_4$ and $N_2$ also sublimate around this temperature. Once the most volatile molecules have evaporated, as the temperature increases, strong modifications related to the band complex between 2200 and 2050 $cm^{-1}$ are still observed. The $CN^-$ and HCN bands disappear progressively and the band complex evolves towards higher frequencies corresponding to nitrile and isonitrile transitions in a solid residue.

The absorbance of the N-H feature between 3500 $cm^{-1}$ and 2400 $cm^{-1}$ increases with the final dose deposited during the irradiation. The same evolution is observed in the nitrile region at 2200 $cm^{-1}$, however, in the region of C=C, C=N, and C-N (at 1650 $cm^{-1}$, 1600 $cm^{-1}$, and 1350 $cm^{-1}$), the most intense spectra are that of samples b and d followed by samples a and c.

The spectra of the room temperature residues of samples a–d are shown in Fig. 9. The spectrum of residue d, after heating to 600 K under primary vacuum, is shown in the same figure. This second annealing was an attempt to reproduce the atmospheric

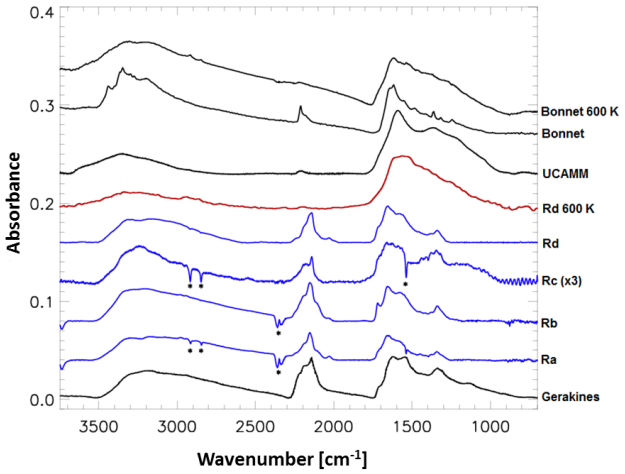


**Fig. 9.** Superposition of FTIR spectra of different residues compared to the spectrum of an UCAMM. *From top to bottom*: poly-HCN before and after annealing to 600 K (Bonnet et al. 2015); spectrum of a UCAMM (Dartois et al. 2013); spectrum of residue "d" of this work, post-annealed to 600 K (in red), spectra of residues "a" to "d" produced in this work after irradiation and annealing to 300 K (in blue); spectrum of pure HCN ice after irradiation with 0.8 MeV protons (Gerakines et al. 2004).

**Table 3.** Infrared absorption bands observed in the residue formed after irradiation, and their attribution.

| Bands | Attribution |
|---|---|
| 3500–2400 $cm^{-1}$ | N-H |
| 2200 $cm^{-1}$ | C≡N |
| 1650 $cm^{-1}$ | C=C |
| 1600 $cm^{-1}$ | C=N |
| 1350 $cm^{-1}$ | C-N |

entry. The main bands identified in the residue are reported in Table 3.

Although sample c was irradiated at a lower total dose (3 eV $molecule^{-1}$), the residue IR spectrum is similar to those obtained for higher doses. The final spectra indicate that even if the evolution of the spectra are different and even if the initial composition are slightly different, the residues are similar.

These results suggest that the raw matter needed to process the residue during annealing is formed starting at the very beginning of the irradiation. The formation process seems to continue during the whole irradiation period. Further experiments will investigate this hypothesis by processing a more important part of the ice, by irradiating the ice at much higher doses. We constrained the minimum and typical required irradiation dose, and cthe corresponding astrophysical timescale, to form a meaningful residue.

## 4. Discussion

### 4.1. Residue formation

Although starting with different initial concentrations and depositing different final doses, the produced residues share similar spectral signatures. If the initial conditions for the starting ice mixtures are different, they all contain $CH_4$ in a $N_2$ dominated matrix, but in varying proportions reflecting the expected chemical diversity of the subsurface of outer solar system bodies (e.g. as mapped on Pluto; Protopapa et al. 2016). As shown in Figs. 3 to 6, the same main molecules and radicals are produced upon ion irradiation, but their amount and the saturation dose change as a result of both the initial molecule concentration and the total deposited doses. The irradiation process produces mainly CN-related species, which are reactive species and easily polymerizable. Consequently, this leads to the synthesis of a rather common residue within the dose regime explored here. At the end of the process, once the nitrogen-rich polyaromatic material is formed, it is expected to stay more resilient to further irradiation. This will be explored in future experiments.

Figure 9 shows the similarity between a spectrum from Gerakines et al. (2004) obtained after low energy proton irradiation of pure HCN ice, two poly-HCN spectra from (Bonnet et al. 2015) and the four residue spectra of this work. The pure HCN residue and both poly-HCN present the same features as listed in Table 3. Moreover, the nitrile band presents a similar relative intensity compared to the C=N region as that of the residues obtained in this work. This indicates that, as stated above, one of the most abundant molecules formed during irradiation is HCN and $CN^-$ and that other molecules present before annealing are contributing less significantly to the residue. Swift heavy ions transform an $N_2$-$CH_4$ ice into a poly-HCN like polymer compound. This is confirmed by ex-situ electron microprobe measurements performed on the residues maintained under primary vacuum, show atomic N/(N+C) ratio of the order of 0.5, supporting the hypothesis of formation of a HCN-like polymer.

The four residues can also be compared to tholins spectra, such as those presented in Bonnet et al. (2015). Such experiments are performed from gaseous products in laboratory reactors at room temperature aimed at produceing nitrogen-rich cometary dust and/or Titan atmosphere analogues. These spectra, produced from $N_2$-$CH_4$ (90:10) starting gas mixtures, are relevant to compare the structure and chemical signatures of analogues with extraterrestrial materials and are a means to to synthesize analogues with the foreseen spectral signatures. These experiments show that the formation of a HCN-like polymer is a stable chemical pathway also expected in a plasma polymerization. Beyond the mere structure of an irradiation-induced analogue, the experiments described in this work are simulating solar system environments and processes that are directly relevant for the formation of the organic compound observed in UCAMMs. Therefore, the starting bricks are simple and elementary, such as relatively ubiquitous simple ices, and processed at low temperature and under high vacuum relevant for outer solar system environments. In the same way, the spectra of the residues shown in Gerakines et al. (2004) are similar, although they are obtained starting with different initial ices. This suggests that a similar residue is obtained when a molecular mixture containing C, N and H is processed by an energetic source. However, the purpose of the present work is to reproduce a realistic astrophysical scenario, leading us to use the simplest possible ices as starting point. A constraint on the irradiation environment is set by the need for energetic processes to make it possible for large amounts of N to be incorporated in the final residue. We emphasize again that a lower volume is affected by UV photons than by energetic ions for large icy bodies. Even if CO is observed in a small amount in the astrophysically targeted object ices and $H_2O$ is present as a contaminant in our experiments leading to small carbonyl contributions, the residues obtained from the irradiations that match the nitrogen-rich organic matter found in UCAMMs imply the absence of large amounts of O or co-mixed $H_2O$ in the starting ices. Much larger initial O content would

lead to very different organic residues and final chemical compositions. All together, these points show that heavy ions are able to process $N_2$-$CH_4$ ices and that annealing of the irradiated ices provides a stable poly-HCN-like residue, in a reasonable astrophysical scenario.

The residues obtained by irradiation of the above ice samples can also be compared with the spectra of an UCAMM (Fig. 9). The similarity between the spectra is striking, as the five major bands observed in the residues are also present in the UCAMM spectrum. There are still differences, such as the intensity of the nitrile and isonitrile region of the spectrum (2250−2100 $cm^{-1}$), which is more important in the residues. As shown in Fig. 1 of Bonnet et al. (2015) and following the vacuum annealing at 600 K of our residue from sample d, however, slight thermal evolution of the poly-HCN and residue at $T$ above 300 K (up to 600 K in our case) produces a better match to UCAMM spectra. This second annealing is performed to simulate the entry of micrometeroites into the atmosphere. Thus the as-produced residues appear as meaningful precursors to UCAMMs.

### 4.2. Timescale

The present work allows us to obtain constraints on the ability to produce the organic matter of UCAMMs or their precursors using simple processes occurring in the solar system. Furthermore, this work also allows us to evaluate the associated timescales to form a precursor of the N-rich UCAMM organic matter from the starting ice material. The cosmic ray dose experienced at large distances in the solar system can be evaluated by modelling their distribution and fluences (Shen et al. 2004).

The ice composition does not significantly change after a dose of 10−20 eV $molecule^{-1}$ (see Fig. 4). The time corresponding to the deposition of this dose may therefore be considered as the time needed to produce a precursor of the N-rich UCAMM organic matter.

In the study reported by Shen et al. (2004) exploring cosmic ray (and secondary UV photons) interactions with icy grains, the mean rate of energy deposition to the ice mantles is on the order of $6 \times 10^{-15}$ eV $molecule^{-1}$ $s^{-1}$. The equivalent timescale to reach an irradiation dose of about 10 eV $molecule^{-1}$ corresponds to about 53 million years, a dose at which an organic residue is already efficiently produced in the experiments presented in this work. This value represents a lower limit to the time needed to produce a solid organic matter precursor. Irradiating for longer times would produce more residues of similar nature (54 eV $molecule^{-1}$, the dose reached for sample b, corresponds to 270 millions years). At large heliocentric distances, interstellar UV photons add their contribution to the formation of a residue, lowering the required timescale at the very near surface. The volume affected by UV photons is much lower for planetesimals or bodies with sizes exceeding their penetration depth (hundreds of nm) as compared to heavy ions, unless they act in the very early stages of the protosolar nebula disk. Typically hundreds of millions year are required to produce a significant amount of residues. The irradiation process can be effective as soon as the N-rich ice mantles were formed. It may have started as soon as the planetesimals were formed, but it can still be ongoing today for bodies at large heliocentric distances, i.e. beyond the "nitrogen snow-line", as discussed in Dartois et al. (2013).

According to Cooper et al. (2003, Table 5), within this timescale, at large heliocentric distances and in the local ISM a radiolytically significant dose can be deposited and affect up to several $\mu$m of ice layer. Although affecting only the top layer, such a process may produce substantial amounts of organic matter in particular for small-to-intermediate size icy bodies in the Oort cloud.

## 5. Conclusion

We irradiated nitrogen-dominated ice mixtures of $N_2$-$CH_4$ (90:10 and 98:2) at 14 K with swift heavy ions. This allows us to simulate modifications induced by cosmic rays on transneptunian to Oort cloud object surfaces. During the irradiation, numerous intermediate species were produced, including predominantly HCN and $CN^-$, but also including HNCO, CO, or $OCN^-$ from traces of water in the matrix. Starting from simple ice mixtures representative of icy surfaces of outer solar system objects, we effectively produce complex molecules and radicals. During the annealing of the irradiated ices to room temperature, these species recombine and react to produce a solid residue. The analysis of the residue confirms the formation of a poly-HCN-like material, which is stable at room temperature. These poly-HCN-like materials are potential precursors of organic material observed in ultracarbonaceaous micrometeorites collected in Antarctica. The associated formation timescales are compatible with an irradiation of icy bodies orbiting in the outer solar system. Further studies should explore in detail the post-irradiation history of such residues when travelling to the internal parts of the solar system.

*Acknowledgements.* This work was supported by the ANR IGLIAS project, grant ANR-13-BS05-0004 of the French Agence Nationale de la Recherche, by the CAPES-COFECUP French-Brazilian exchange programme. M.G., C.E. and J.D. acknowledge financial support from the ANR project OGRESSE (11-BS56-026-01) and DIM-ACAV. E.D. acknowledge financial support by the French INSU-CNRS programme "Physique et Chimie du Milieu Interstellaire" (PCMI). The Brazilian agencies CNPq (INEspaço and Science without Borders) and FAPERJ are also acknowledged. We thank T. Been, C. Grygiel, T. Madi, I. Monnet, F. Ropars and J.M. Ramillion for their invaluable support. We also thank the anonymous reviewer for constructive remarks on this work.

## References

Baratta G. A., Chaput. D., Cottin. H., et al. 2015, Planet. Space Sci., 118, 211
Bennett, C. J., Jamieson, C. S., Osamura, Y., & Kaiser, R. I. 2006, ApJ, 653, 792
Bentwood, R. M., Barnes, A. J., & Orville-Thomas, W. J. 1980, J. Mol. Spectr., 84, 391
Bonnet, J. Y., Quirico, E., Buch, A., et al. 2015, Icarus, 250, 53
van Broekhuizen, F. A., Keane, J. V., & Schutte, W. A. 2004, A&A, 415, 425
Burgdorf, M., Cruikshank, D. P., Dalle Ore, C. M., & Sekiguchi, T. 2010, ApJ, 718, L53
Cooper, J. F., Christian, E. R., Richardson, J. D., & Wang, C. 2003, Earth Moon and Planets, 92, 261
Cruikshank, D. P., Grundy, W. M., DeMeo, F. E., et al. 2015, Icarus, 246, 82
Dartois, E., Engrand, C., Brunetto, R., et al. 2013, Icarus, 224, 243
Derenne, S., & Robert, F. 2010, Meteoritics and Planetary Science, 45, 1461
Dobrică, E., Engrand, C., Leroux, H., Rouzaud, J. N., & Duprat, J. 2012, Geochim. Cosmochim, 76, 68
Dobrică, E., Engrand, C., Quirico, E., Montagnac, G., & Duprat, J. 2011, Meteoritics and Planetary Science, 46, 1363
Duprat, J., Dobrică, E., Engrand, C., et al. 2010, Science, 328, 742
Duprat, J., Engrand, C., Maurette, M., et al. 2007, Adv. Space Res., 39, 605
Ebihara, M., Sekimoto, S., Shirai, N., et al. 2013, Lunar and Planetary Science Conference, 44, 2086
Ehrenfreund, P., Robert, F., d'Hendecourt, L., & Behar, F. 1991, A&A, 252, 712
Engrand, C., Benzerara, K., Leroux, H., et al. 2015, Lunar and Planetary Science, 46, 1902
Escobar, A., Giuliano, B. M., Muñoz Caro, G. M., Cernicharo, J., & Marcelino, N. 2014, ApJ, 788, 19
Gerakines, P. A., Bray, J. J., Davis, A., & Richey, C. R. 2005, ApJ, 620, 2240
Gerakines, P. A., Moore, M. H., & Hudson, R. L. 2004, Icarus, 170, 202
Greenberg, J. M., Li, A., Mendoza-Gomez, C. X., et al. 1995, ApJ, 455, L177
Grundy, W. M., Binzel, R. P., Buratti, B. J., et al. 2016, Science, 351, 9189

Hammer, P., Victoria, N. M., & Alvarez, F. 2000, Journal of Vacuum Science and Technology A, 18, 2277
Hudson, R. L., Moore, M. H., & Gerakines, P. A. 2001, ApJ, 550, 1140
Jheeta, S., Domaracka, A., Ptasinska, S., Sivaraman, B., & Mason, N. J. 2013, Chem. Phys. Lett., 556, 359
Kebukawa, Y., Alexander, C. M. O. D., & Cody, G. 2010, Geochim. Cosmochimi. Acta, 75, 3530
Kitajima, F., Nakamura, T., Takaoka, N., & Murae, T. 2002, Geochim. Cosmochimi. Acta, 66, 163
Levi, A., & Podolak, M. 2011, Icarus, 214, 308
Licandro, J., Grundy, W. M., Pinilla-Alonso, N., & Leisy, P. 2006, A&A, 458, L5
Lorenzi, V., Pinilla-Alonso, N., & Licandro, J. 2015, A&A, 577, A86
Moon, E. S., Kang, H., Oba, Y., Watanabe, N., & Kouchi, A. 2010, ApJ, 713, 906
Moore, M. H., & Hudson, R. L. 2003, Icarus, 161, 486
Muñoz Caro, G. M., & Dartois, E. 2013, Chem. Soc. Rev., 42, 2173
Muñoz Caro, G. M., Meierhenrich, U., Schutte, W. A., Thiemann, W. H. P., & Greenber, J. M. 2004, A&A, 413, 209
Nakamura, T., Imae, N., Nakai, I., et al. 1999, Antarctic Meteorite Research, 12, 183
Nakamura, T., Noguchi, T., Ozono, Y., Osawa, T., & Nagao, K. 2005, Meteoritics and Planetary Science Supplement, 40, 5046
Nuevo, M., Meierhenrich, U., Muñoz Caro, G. M., & Dartois, E 2006, A&A, 457, 741
Ong, C. W., Zhao, X. A., Tsang, Y. C., Choy, C. L., & Chan, P. W. 1996, Appl. Phys. A, 280, 1
Orthous-Daunay, F. R., Quirico, E., Beck, P., et al. 2013, Icarus, 223, 534
Palumbo, M. E., & Strazzulla, G. 1993, A&A, 269, 568
Pilling, S., Seperuelo Duarte, E., da Silveira, E. F., et al. 2010, A&A, 509, A87
Protopapa, S., Berry, K. L., Binzel, R. P., et al. 2016, 47th Lunar and Planetary Science Conf., 47, 2815
Quirico, E., Montagnac, G., Lees, V., McMillan, P. F., et al. 2008, Icarus, 198, 218
Remusat, L., Robert, F., & Derenne, S. 2007, Comptes rendus Géosiences, 339, 895
Rodil, S. E., Ferrari, A. C., Robertson, J., & Milne, W. I. 2001, J. Appl. Phys., 89, 5425
Satorre, M. Á., Domingo, M., Millán, C., et al. 2008, Planetary and Space Science, 46, 1748
Seperuelo Duarte, E., Boduch, P., Rothard, H., et al. 2009, A&A, 502, 599
Schaller, E. L., & Brown, M. E. 2007, ApJ, 659, L61
Shen, C. J., Greenberg, J. M., Schutte, W. A., & van Dishoeck, E. F. 2004, A&A, 415, 203
Yabuta, H., Itoh, S., Noguchi, T., et al. 2012, Lunar and Planetary Science Conf., 43, 2239
Ziegler, J. F., Ziegler, M. D., & Biersack, J. P. 2010, Nuclear Instruments and Methods in Physics Research B, 268, 1818